RSC Advances

PAPER

View Article Online
View Journal | View Issue

Cite this: *RSC Adv.*, 2019, **9**, 27050

The dynamic CO_2 adsorption of polyethylene polyamine-loaded MCM-41 before and after methoxypolyethylene glycol codispersion†

Xia Wang, *[a] Wulan Zeng,[a] Hongyan Zhang,[a] Dan Li,[a] Hongjing Tian,[b] Xiude Hu,[c] Qian Wu, *[a] Chunling Xin,*[a] Xiaoyu Cao[a] and Wenjing Liu[a]

To reduce the cost of CO_2 capture, polyethylene polyamine (PEPA), with a high amino density and relatively low price, was loaded into MCM-41 to prepare solid sorbents for CO_2 capture from flue gases. In addition, methoxypolyethylene glycol (MPEG) was codispersed and coimpregnated with PEPA to prepare composite sorbents. The pore structures, surface functional groups, adsorption and regeneration properties for the sorbents were measured and characterized. When CO_2 concentration is 15%, for 30, 40 and 50 wt% PEPA-loaded MCM-41, the equilibrium adsorption capacities were respectively determined to be 1.15, 1.47 and 1.66 mmol g^{-1} at 60 °C; for 30 wt% PEPA and 20 wt% MPEG, 40 wt% PEPA and 10 wt% MPEG, and 50 wt% PEPA and 5 wt% MPEG codispersed MCM-41, the equilibrium adsorption capacities were respectively determined to be 1.97, 2.22 and 2.25 mmol g^{-1} at 60 °C; the breakthrough and equilibrium adsorption capacities for 50 wt% PEPA and 5 wt% MPEG codispersed MCM-41 respectively reached 2.01 and 2.39 mmol g^{-1} at 50 °C, all values showed a significant increase compared to PEPA-modified MCM-41. After 10 regenerations, the equilibrium adsorption capacity for codispersed MCM-41 was reduced by 5.0%, with the regeneration performance being better than that of PEPA-loaded MCM-41, which was reduced by 7.8%. The CO_2-TPD results indicated that the mutual interactions between PEPA and MPEG might change basic sites in MCM-41, thereby facilitating active site exposure and CO_2 adsorption.

Received 15th July 2019
Accepted 23rd August 2019

DOI: 10.1039/c9ra05404a

rsc.li/rsc-advances

1. Introduction

Coal-fired power plants are undoubtedly large CO_2 emission points all over the world, in which the capture of CO_2 has been extensively researched; Bui *et al.* has reviewed the progress for carbon capture and storage (CCS) and pointed out the way forward.[1–3] Solid amine adsorption technology, with weak corrosivity, highly efficient adsorption performance and low regeneration energy consumption, is recognized as an effective method.[4–7]

So far the study of amine-loaded solid sorbents mainly focuses on immobilizing amines onto the inner surface of porous supporting materials, such as metal–organic frameworks (MOFs),[8–13] mesoporous molecular sieves,[14–22] silicas[23–31] and so on.[32–40] Chen *et al.* incorporated polyethyleneimine (PEI) into mesoporous zeolite 13X prepared by pore-expanding original micropores; due to PEI-dispersion in mesopores, the CO_2 adsorption capacity for PEI-modified 13X reached 80 mg g^{-1} at 100 °C under a pure CO_2 atmosphere.[16] Saha immobilized PEI in silicas and polymethyl methacrylate (PMMA) to prepare type I adsorbents, grafted different amounts of aminosilanes in mesoporous SBA-15 to prepare type II adsorbents and performed breakthrough adsorption experiments. Both sorbents showed significant adsorption capacities and consistent regenerability during 3–5 adsorption–desorption cycles.[5] Cheng *et al.* incorporated amines into silicas with trimodal pore structures, and the nanocomposite sorbents suggested rapid adsorption kinetics and good adsorption performance, with an adsorption capacity of 172 mg g^{-1} being obtained for an amine loading amount of 70 wt%.[25] To further improve the dispersion and stability of TEPA or PEI with high viscosity, auxiliary reagents with hydroxyl or ether groups were coloaded into supporting materials for preparing composite sorbents.[41–44] Jung *et al.* coimpregnated PEI and 1,3-butadienediepoxide (BDDE) with hydroxyl groups in silicas to investigate the improved CO_2 adsorption performance of PEI-loaded silicas, which was primarily attributed to following two aspects. On the one hand, synergistic combinations between hydroxyl groups and the PEI on the inner surface of the supporting materials occurred, which promoted the dispersion and thermostability of PEI in silicas. On the other hand, after coimpregnation, the chemisorption ratio for amine and CO_2 molecules changed

[a]Department of Chemistry and Chemical Engineering, Weifang University, Weifang 261061, Shandong, China. E-mail: xiawangwfu@163.com
[b]College of Chemical Engineering, Qingdao University of Science & Technology, Qingdao 266042, China
[c]State Key Laboratory of High-Efficiency Utilization of Coal and Green Chemical Engineering, Ningxia University, Yinchuan 750021, China

† Electronic supplementary information (ESI) available. See DOI: 10.1039/c9ra05404a

from 2 : 1 to 1 : 1, and the CO_2 adsorption efficiency improved.[41] Mafra *et al.* performed two-dimensional solid-state nuclear magnetic resonance (NMR) experiments on amine-modified silicas after adsorbing CO_2; the results showed that all chemisorbed CO_2 molecules participated in hydrogen bonding interactions with either neighboring alkylamines or surface silanols, and the work helped one to understand the configuration of chemisorbed CO_2.[27] Afonso *et al.* prepared primary amine-modified mesoporous silicas and performed NMR experiments; different conformations of carbamic acid, alkylammonium carbamate as well as hydrogen bonds were confirmed using a density functional theory (DFT) model. The study also provided well understanding of the chemisorbed CO_2 in amine-oxide hybrid surfaces at a molecular-level.[28]

In this work, PEPA, with similar amino density but a lower price than tetraethylenepentamine (TEPA) and PEI (the price for PEPA, TEPA and PEI were respectively ¥68 per 500 mL, ¥199 per 500 mL and ¥1199 per 500 mL), was impregnated into mesoporous MCM-41 to prepare solid amine sorbents, and MPEG was also codispersed with PEPA to prepare composite sorbents. The pore structures, surface functional groups and desorption properties for MCM-41 before and after loading were characterized; the adsorption and regeneration performances were also studied. In addition, the improvement in the adsorption performance of PEPA-loaded MCM-41 due to the MPEG was also discussed.

2. Experimental

2.1 Materials

MCM-41 was provided by the Tianjin Nanhua Catalyst Company in China, polyethylene polyamine (PEPA) and methoxypolyethylene glycol (MPEG) were bought from Shanghai Aladdin Bio-Chem Technology Co., Ltd in China, and anhydrous ethanol was supplied by Sinopharm Chemical Reagent Co., Ltd in China. N_2 (99.999%) and the simulated flue gas, with a volume ratio of 85% N_2 (99.999%) to 15% CO_2 (99.999%), were distributed by the Anqiu Hengan Gas Factory.

2.2 Preparation of PEPA-loaded MCM-41 before and after MPEG codispersion

The preparation of PEPA-loaded MCM-41 adopted a wet impregnation method under ultrasound-assistance.[15] A calculated volume of PEPA was dissolved in anhydrous ethanol in a beaker, with the solution being sonicated for 30 min; then, MCM-41 with a mass of 1.0 g was quickly added and the beaker was continuously sonicated for another 120 min. The mixture was dried in an electric drying oven at 90 °C for 24 h and named as MCM-41-PEPA*a*, where *a* is the weight loading amount of PEPA in the sorbent.

For PEPA and MPEG codispersed MCM-41, the preparation process was as above, and a calculated amount of PEPA and MPEG were first codispersed in anhydrous ethanol before impregnating into MCM-41. The corresponding composite sorbents were named as MCM-41-PEPA*a*-M*b*, with M representing MPEG and *a*, *b* separately representing the weight loading amounts of PEPA, MPEG in the composite sorbents.

2.3 Characterization

The N_2 adsorption–desorption isotherms for PEPA-loaded MCM-41 before and after MPEG codispersion were performed using an ASAP 2460 (Micromeritics, America) at an analysis bath temperature of 77 K. The BET surface area was measured and calculated by the Brunauer–Emmett–Teller (BET) equation; the pore volume was estimated from the N_2 adsorption amount at a relative pressure of $P/P_0 = 0.99$; the pore size distribution curves were determined from the Barrett–Joyner–Halenda (BJH) desorption branch.

The surface functional groups for PEPA-loaded MCM-41 before and after MPEG codispersion were measured using Fourier-transform infrared spectroscopy (FT-IR) with a TENSOR-27 (Bruker, Germany) over a frequency range of 4000 to 500 cm^{-1}.

X-ray diffraction patterns were collected using the ASAP 2020 V4.01 X-ray diffractometer with Cu Ka radiation ($\lambda = 0.154$ nm) in the range of $2\theta = 10 - 80°$.

Temperature-programmed desorption (TPD) experiments were conducted using a fully automatic multipurpose instrument: a TP-5080 (Xianquan, China). CO_2 adsorption was performed at 60 °C, and then the temperature was elevated at a rate of 10 K min^{-1} in N_2.

The thermostability for TEPA and PEPA was determined using a NETZSCH, STA 449F3 (Netzsch, Germany). 10 milligrams of the sample was placed in an alumina pan and N_2 was passed at a flow rate of 40 mL min^{-1} at room temperature; then, the temperature was heated to 700 °C at a rate of 10 K min^{-1}.

2.4 CO_2 adsorption and regeneration experiments

CO_2 adsorption and regeneration experiments were performed on our self-assembled fixed-bed reactor, in which the inner diameter and length of the quartz tube were 0.8 and 40 cm, respectively.[18] The sorbent with a weight of 1.0 g was filled into the reactor, and N_2 was passed in at a flow rate of 30 mL min^{-1}; then, the temperature was increased to 100 °C and held constant for 60 min; the temperature was then decreased to a certain adsorption temperature, and the inlet gas was switched to the simulated flue gas with a flow rate of 30 mL min^{-1}, where in the CO_2 adsorption process began. Meanwhile, the CO_2 concentration at the reactor outlet (C) was detected by on-line gas chromatography. When C doesn't change and equals the CO_2 concentration at the inlet (C_0), an adsorption process finishes, which is called equilibrium adsorption stage, with the adsorption amount at this stage being the equilibrium adsorption capacity; when C is equal to 5% of C_0, a breakthrough adsorption stage is reached, in which the adsorption time and amount are called the breakthrough time and breakthrough adsorption capacity. The adsorption capacity was integrally calculated from the breakthrough curve as discussed previously.[15]

After completing the equilibrium adsorption, the inlet gas was switched to N_2 and the temperature was increased to 100 °C to perform the desorption process. When CO_2 was not checked at the outlet, the desorption process was completed and the

sorbent was regenerated. Ten adsorption–desorption regenerations were performed in this study.

3. Results and discussions

3.1 Characterization

3.1.1 N_2 adsorption–desorption. The N_2 adsorption–desorption isotherms and pore size distribution curves for MCM-41 before and after loading are shown in Fig. 1, and the BET surface area, total pore volume as well as average pore size are shown in Table 1. As seen in Fig. 1(a), for MCM-41 and MCM-41-PEPA30%, the isotherms suggested a type IV adsorption and hysteric loops suggested a H3 type adsorption, capillary condensation below a relative pressure of 0.4 appeared, showing a mesopore structure for MCM-41 before and after functionalization; for MCM-41-PEPA50% before and after MPEG codispersion, the hysteric loops and capillary condensation phenomenon almost disappeared, showing that most channels were taken up by active components. From Fig. 1(b), the pore size for MCM-41 centered at 2.8 and 3.9 nm, while for MCM-41-PEPA30%, the pores centered at 2.8 nm almost disappeared, suggesting that the active components preferentially entered relatively small mesopores. As seen from Table 1, the introduction of active components reduced the surface area and pore volume of MCM-41, but for MCM-41-PEPA50% and MCM-41-PEPA50%-M5%, partial pores still remained, which could provide channels for the transfer and capture of CO_2.

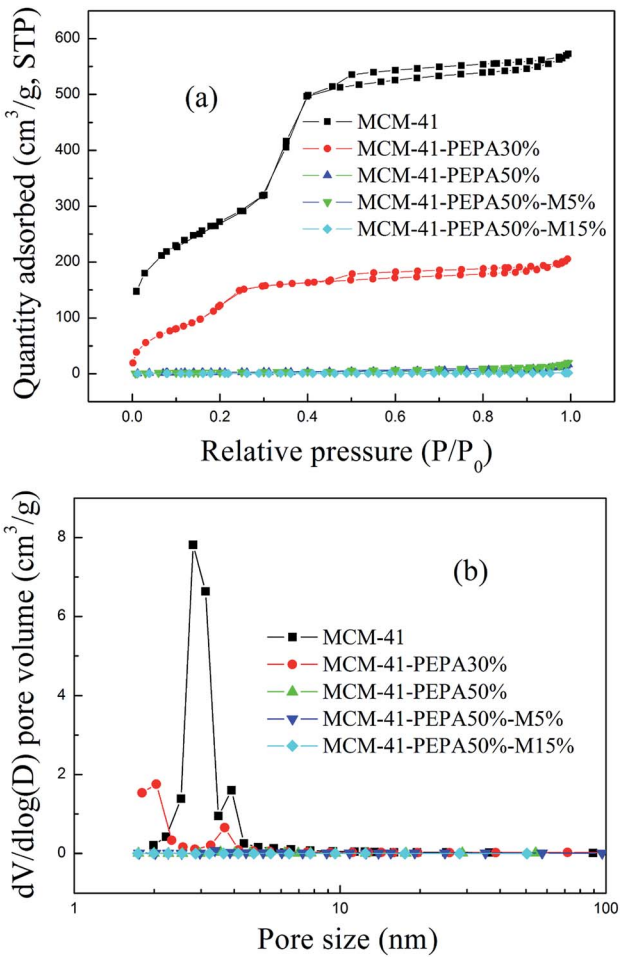

Fig. 1 (a) N_2 adsorption–desorption isotherms and (b) pore size distribution curves for MCM-41 before and after loading.

3.1.2 FT-IR spectra. The FT-IR spectra for MCM-41 before and after PEPA and MPEG codispersion are shown in Fig. 2. Comparing with MCM-41, MCM-41-PEPA50% showed the bending and symmetric stretching vibrations of N–H from primary amine at 1564 and 1480 cm^{-1}, respectively, the stretching vibrations of C–N from primary or secondary amine at 1230 cm^{-1}, as well as weak stretching vibrations of C–N from tertiary amine at 1317 cm^{-1}, meaning that PEPA was loaded into MCM-41 *via* the wet impregnation method.[15,45] Comparing with MCM-41-PEPA50%, MCM-41-PEPA50%-M5% appeared distinct symmetric and asymmetric stretching vibrations of C–H from the alkyl groups at 2950 and 2840 cm^{-1}, as well as enhanced characteristic peak at 1230 cm^{-1}, which is caused from the asymmetric stretching vibrations of C–O–C in the aliphatic ether or the bending vibrations of C–O–H, suggesting that MPEG was also introduced into MCM-41.[42,45] In addition, the peaks characterizing PEPA all obviously enhanced, which is an indication that MPEG promoted the dispersion and exposure of PEPA in the pore channels of MCM-41.

3.1.3 Thermostability. According to previous studies, TEPA-modified mesoporous sorbents suggested good thermostability at a desorption temperature of 100 °C.[18,40] The thermal gravimetric curves for PEPA and TEPA were measured under the same conditions and are shown in Fig. 1S in the ESI.† As seen in Fig. 1S,† PEPA and TEPA exhibited almost coincident curves below 140 °C, therefore, PEPA-loaded MCM-41 showed a similar thermostability to TEPA-modified MCM-41, which was also thermodynamically suitable for application in adsorption and regeneration processes.

3.1.4 XRD. The XRD patterns for MCM-41, MCM-41-PEPA50% and MCM-41-PEPA50%-M5% are shown in Fig. 2S.† MCM-41 appeared a broad peak at $2\theta = 24.1°$; for MCM-41-PEPA50% before and after MPEG codispersion, the characteristic peak retained, but suggested a slight shift to the left, showing that the active components were dispersed into the inner surface of MCM-41, and mutual interactions occurred. Similar phenomenon was also reported previously.[15]

3.2 PEPA-loaded MCM-41 for CO_2 adsorption

3.2.1 The effect of the PEPA loading ratio. Different weight ratios of PEPA-loaded MCM-41 were prepared and studied for CO_2 adsorption at 60 °C, and breakthrough adsorption curves along with adsorption capacity data are demonstrated in Fig. 3. As seen in Fig. 3(a), as the PEPA loading was increased, the breakthrough curve shifted towards the right, and the breakthrough time became longer, suggesting improved breakthrough and equilibrium adsorption performance for PEPA-loaded MCM-41 when the PEPA-loading was increased from 30–60%. For MCM-41-PEPA50%, breakthrough time, breakthrough and equilibrium adsorption capacities were 6 min, 1.21 and 1.66 mmol g^{-1}, respectively; for MCM-41-PEPA60%, the

Table 1 The pore structure data for MCM-41 before and after loading

Sorbent	BET surface area ($m^2\ g^{-1}$)	Total pore volume ($cm^3\ g^{-1}$)	Average pore size (nm)
MCM-41	956.15	0.98	3.10
MCM-41-PEPA30%	545.21	0.31	2.30
MCM-41-PEPA50%	10.23	0.023	8.91
MCM-41-PEPA50%-M5%	11.34	0.027	9.68
MCM-41-PEPA50%-M15%	2.33	0.0026	4.39

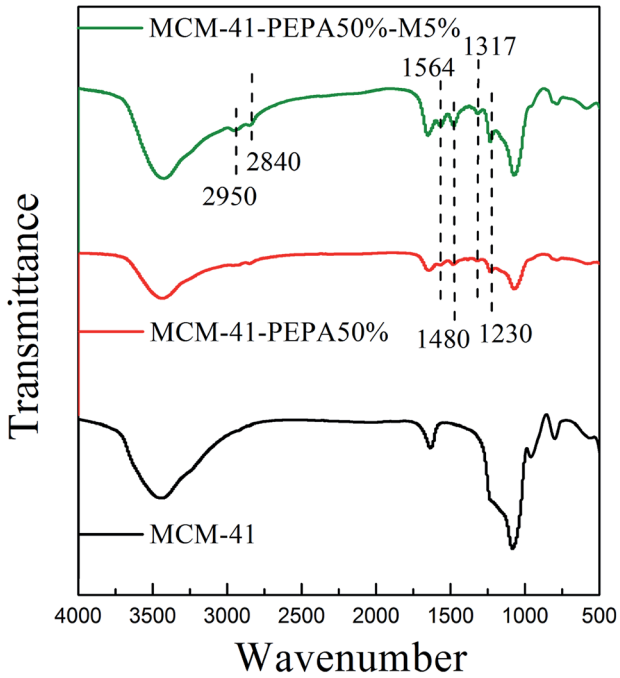

Fig. 2 The FT-IR spectra for MCM-41 before and after PEPA and MPEG codispersion.

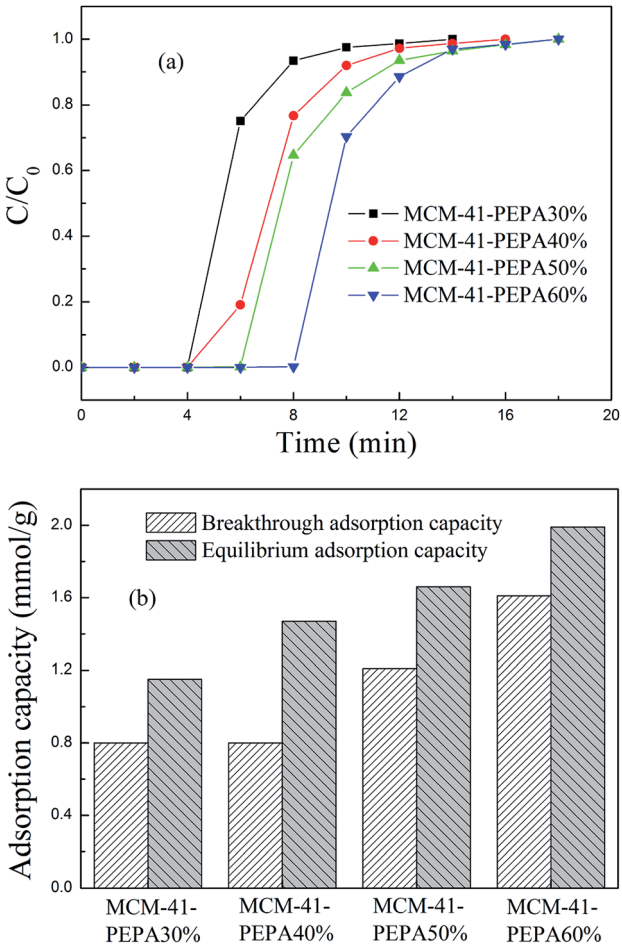

Fig. 3 The (a) breakthrough adsorption curves and (b) adsorption capacities for PEPA-loaded MCM-41 at 60 °C.

corresponding values were 8 min, 1.61 and 1.99 mmol g^{-1}, respectively, with the adsorption performance being comparable with that of TEPA-modified MCM-41 under the same operating conditions.[42] Accordingly, the PEPA, with also a high amino density but lower price than TEPA, is more suitable for use as a primarily active component for CO_2 chemisorption.

3.2.2 The effect of adsorption temperature. The breakthrough adsorption curves for MCM-41-PEPA50% at 30–80 °C were measured and are shown in Fig. 4(a), with the corresponding breakthrough and equilibrium adsorption capacities being shown in Fig. 4(b). As the temperature was increased, the breakthrough and equilibrium adsorption performance for MCM-41-PEPA50% first increased and then decreased, exhibiting a distinct chemisorption characteristic.[46] High temperature favors not only the dispersal of viscous PEPA in the pore channels of MCM-41 but also CO_2 flow and collision with exposed active sites, which facilitates CO_2 adsorption on PEPA-loaded MCM-41.[15,42] However, adsorption is thermodynamically exothermic, and conversely, high temperature hinders CO_2 adsorption. Therefore, the adsorption performance for PEPA-loaded MCM-41 first increased and then decreased as the temperature was increased; the optimal adsorption temperature, breakthrough and equilibrium adsorption capacity were 60 °C, 1.21 and 1.66 mmol g^{-1}, respectively.

3.3 PEPA and MPEG codispersed MCM-41 for CO_2 adsorption

3.3.1 The effect of the MPEG mass ratio on PEPA. Different mass ratios of PEPA and MPEG were codispersed in MCM-41 to discuss the effect of MPEG on the adsorption performance of PEPA-loaded MCM-41 at 60 °C, with the breakthrough adsorption curves and adsorption capacities demonstrated in Fig. 5–7. For MCM-41-PEPA30%, MCM-41-PEPA40% and MCM-41-

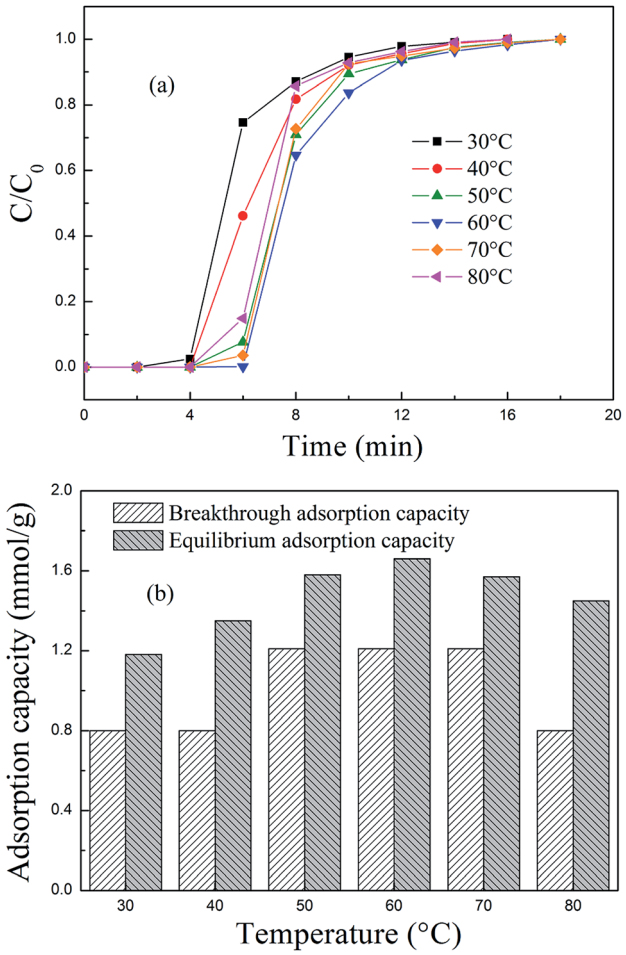

Fig. 4 The (a) breakthrough adsorption curves and (b) adsorption capacities for MCM-41-PEPA50% at different adsorption temperatures.

PEPA50%, the introduction of MPEG caused all breakthrough curves to move towards the right, and breakthrough and equilibrium adsorption performance increased. For MCM-41-PEPA30%-M20%, the breakthrough and equilibrium adsorption capacities were respectively 1.21 and 1.97 mmol g^{-1}, which were improved by 51% and 71% compared to the corresponding values for MCM-41-PEPA30%; for MCM-41-PEPA40%-M10%, the breakthrough and equilibrium adsorption capacities were respectively 1.61 and 2.22 mmol g^{-1}, which were improved by 101% and 51% compared to the corresponding values for MCM-41-PEPA40%; for MCM-41-PEPA50%-M5%, the breakthrough and equilibrium adsorption capacities were respectively 1.61 and 2.25 mmol g^{-1}, which were improved by 37% and 40% compared to the corresponding values for MCM-41-PEPA50%. To sum up, the codispersion of MPEG improved the adsorption performance for PEPA-loaded MCM-41, which might be caused by the hydrogen bonding interactions between the ether groups and hydroxyl groups from MPEG with the amino groups from PEPA, and similar phenomenon has also been reported.[41,43] The hydrogen bonding interactions are expressed as follows.

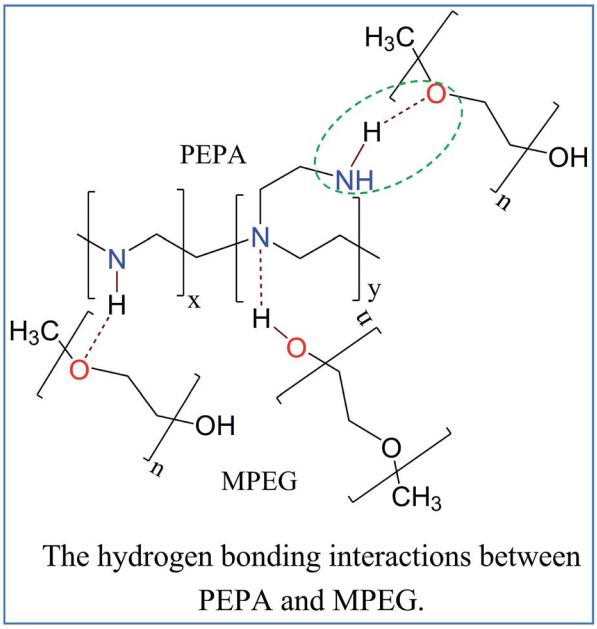

The hydrogen bonding interactions between PEPA and MPEG.

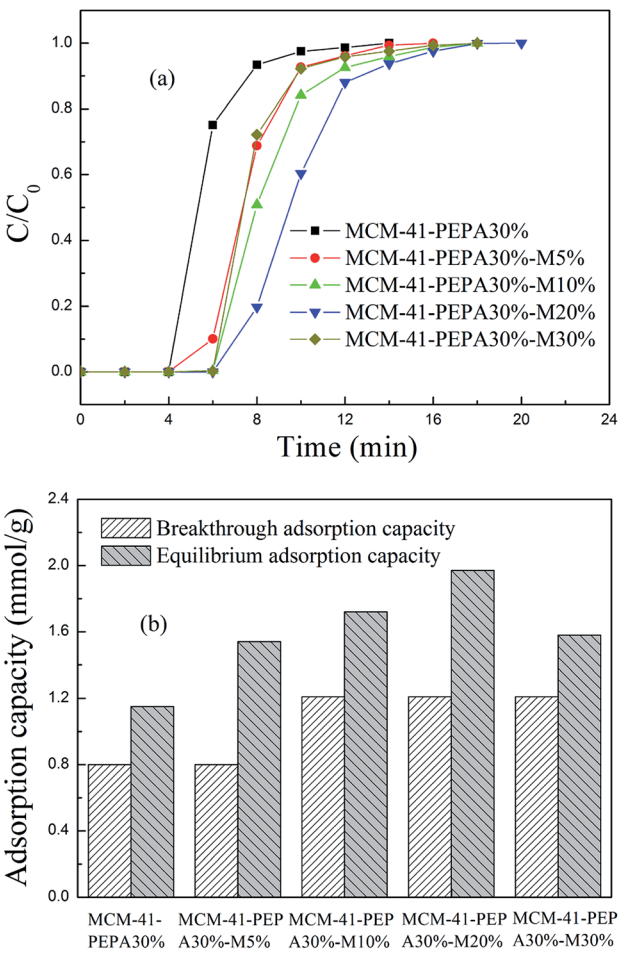

Fig. 5 The (a) breakthrough adsorption curves and (b) adsorption capacities for 30 wt% PEPA and different ratios of MPEG codispersed MCM-41 at 60 °C.

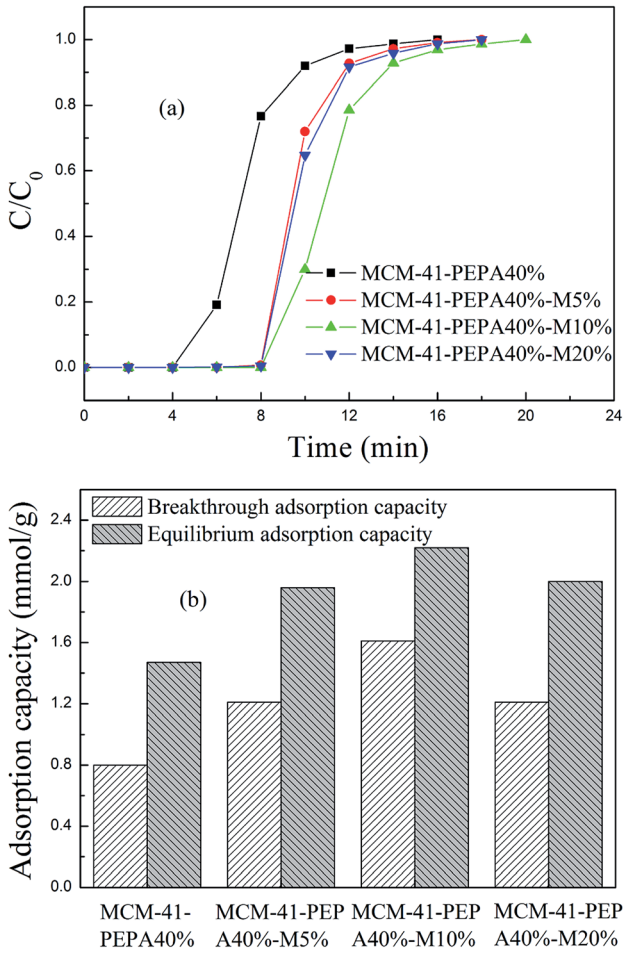

Fig. 6 The (a) breakthrough adsorption curves and (b) adsorption capacities for 40 wt% PEPA and different ratios of MPEG codispersed MCM-41 at 60 °C.

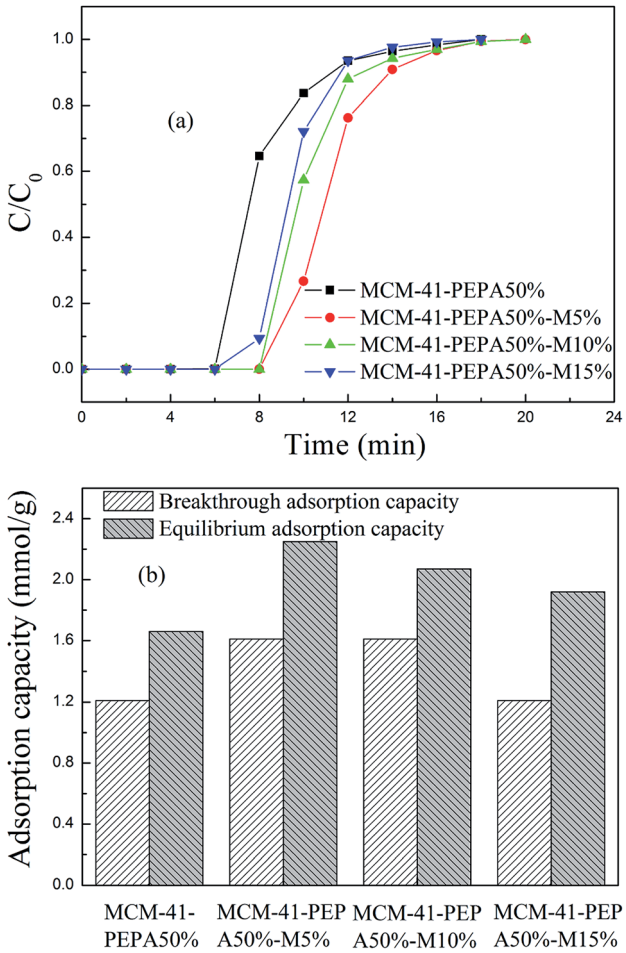

Fig. 7 The (a) breakthrough adsorption curves and (b) adsorption capacities for 50 wt% PEPA and different ratios of MPEG codispersed MCM-41 at 60 °C.

However, the increasing of MPEG didn't cause the adsorption performance for PEPA-loaded MCM-41 to improve continuously, but showed a gradual reduction. MPEG improved the dispersion of easily agglomerated PEPA into the pore channels of MCM-41, but too much MPEG addition could also lead to channel blockage and a decrease in adsorption performance. Among the studied sorbents, 50 wt% PEPA and 5 wt% MPEG codispersed MCM-41 showed good adsorption performance at 60 °C.

3.3.2 The effect of adsorption temperature. Considering the good adsorption performance at 60 °C, the breakthrough curves and adsorption capacities for MCM-41-PEPA50%-MPEG5% at different temperatures were investigated and are shown in Fig. 8. As the temperature was increased, the breakthrough curve first moved towards the right and then the left; so, the corresponding breakthrough and equilibrium adsorption capacities first increased and then decreased, which is also a distinct chemisorption characteristic. The optimum adsorption performance for MCM-41-PEPA50%-M5% appeared at 50 °C, which is lower than that of MCM-41-PEPA50%. The possible explanation for this was that the hydrogen bonding interactions between PEPA and MPEG improved the dispersion and exposure of active amino groups, so the optimal adsorption temperature decreased to a more thermodynamic point. At 50 °C, the breakthrough and equilibrium adsorption capacity for MCM-41-PEPA50%-M5% was 2.01 and 2.39 mmol g^{-1}, respectively, which was increased by 66% and 51% compared to the corresponding values for MCM-41-PEPA50%.

3.4 Regeneration

MCM-41-PEPA50% and MCM-41-PEPA50%-M5% were selected to further investigate the regenerability during 10 adsorption–desorption cycles. The adsorption temperatures for MCM-41-PEPA50% and MCM-41-PEPA50%-M5% were respectively 60 and 50 °C, and the desorption temperatures were all 100 °C, which were set according to previous studies.[40] The equilibrium adsorption capacity data *versus* cycle number figures are depicted in Fig. 9. For both sorbents, the adsorption capacity remained stable during the first three cycles, and then showed a slight decrease. After 10 regenerations, the equilibrium adsorption capacity for MCM-41-PEPA50%-M5% was reduced by 5.0% compared to the fresh sorbent, being better than the

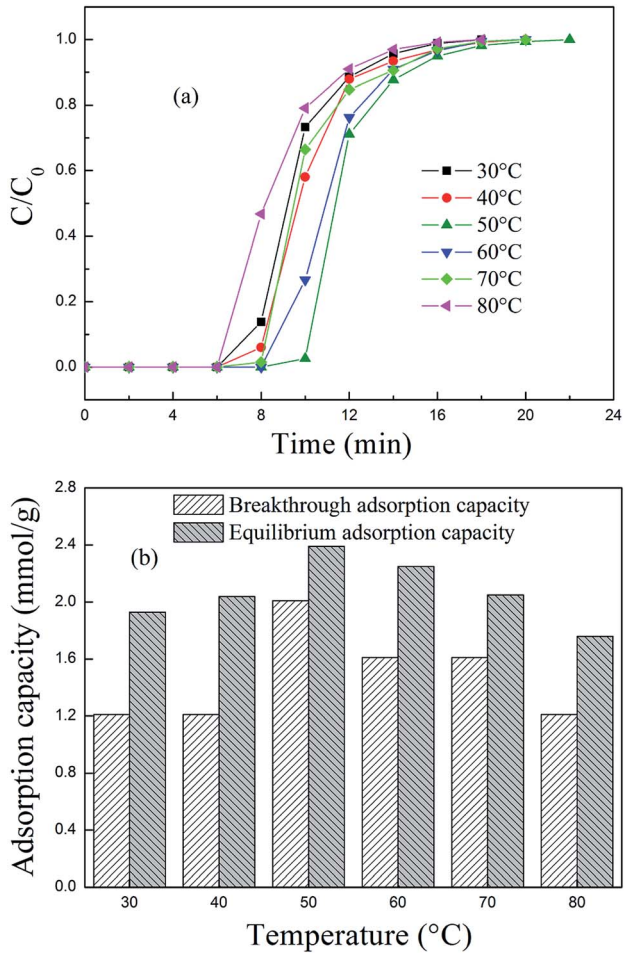

Fig. 8 The (a) breakthrough adsorption curves and (b) adsorption capacities for MCM-41-PEPA50%-M5% at different adsorption temperatures.

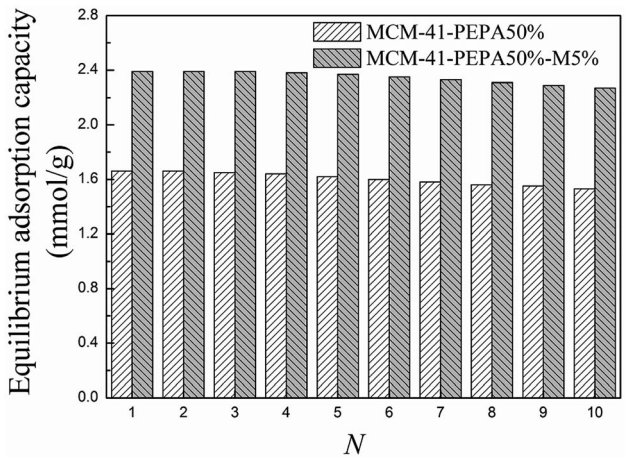

Fig. 9 The equilibrium adsorption capacities for MCM-41-PEPA50% and MCM-41-PEPA50%-M5% during 10 adsorption–desorption cycles.

corresponding value of 7.8% for MCM-41-PEPA50%. Thus, the introduction of MPEG improved the regenerability for PEPA-loaded MCM-41; the reason for this was attributed to the synergistic interactions between functional groups. The synergistic interactions enhanced the stability of PEPA in MCM-41, which reduced its loss during regenerations.

The FT-IR and XRD spectra for MCM-41-PEPA50%-M5% before and after 10 cycles are shown in Fig. 3S and 4S.† Comparing with fresh MCM-41-PEPA50%-M5%, the characteristic peaks for the regenerated sample still retained, suggesting a good regenerability of MCM-41-PEPA50%-M5%; but the peak intensity showed slight decrease, which was due to the evaporation or degradation of the active composites during regenerations. The phenomenon was in accordance with the results from Fig. 9.

3.5 Adsorption and desorption kinetics

3.5.1 Adsorption kinetics. The adsorption rate curves for MCM-41-PEPA50% at 60 °C and MCM-41-PEPA50%-M5% at 50 °C are shown in Fig. 10(a). For both sorbents, the rate curves showed two stages, with a rapid adsorption stage following a relatively slow stage; the point corresponding to the breakthrough adsorption time was determined to be the boundary point of two stages. The rapid stage corresponds to the breakthrough adsorption process, with the rate being 0.20 mmol g^{-1} min^{-1}; for MCM-41-PEPA50%, the adsorption capacity in the rapid stage was 1.21 mmol g^{-1}, accounting for 73% of the equilibrium adsorption capacity, while for MCM-41-PEPA50%-M5%, the adsorption capacity in the rapid stage was 2.01 mmol g^{-1}, accounting for 84% of the equilibrium adsorption capacity, with this value being much higher than that obtained for MCM-41-PEPA50%. In view of the adsorption efficiency, the sorbents are usually regenerated after completing the breakthrough stage. Therefore, the addition of MPEG improved the adsorption efficiency and kinetics for PEPA-loaded MCM-41.

3.5.2 Temperature programmed desorption (TPD) experiments. The TPD curves for MCM-41-PEPA50% and MCM-41-PEPA50%-M5% are shown in Fig. 10(b). In MCM-41-PEPA50%, a weak desorption peak at 80 °C and a strong desorption peak at 117 °C appeared, which corresponded to physisorbed and chemisorbed CO_2, respectively; there is only one kind of basic site in PEPA-loaded MCM-41: the amino groups from PEPA.

In MCM-41-PEPA50%-M5%, two strong desorption peaks appeared at both 80 and 117 °C, suggesting that the addition of MPEG changed the basic sites in the sorbents. In addition to the original amino sites from PEPA, other basic sites appeared at a much lower temperature of 80 °C, which were the amino groups participating in the hydrogen bonding interactions with the ether and hydroxyl groups from MPEG. The hydrogen bonding interactions helped with the dispersion and exposure of the amino groups, and the optimum adsorption temperature for codispersed MCM-41 was reduced to 50 °C. The CO_2-TPD results also confirmed the mutual interactions between PEPA and MPEG, with similar phenomenon previously reported for $NaNO_3$-promoted MgO for CO_2 capture.[47]

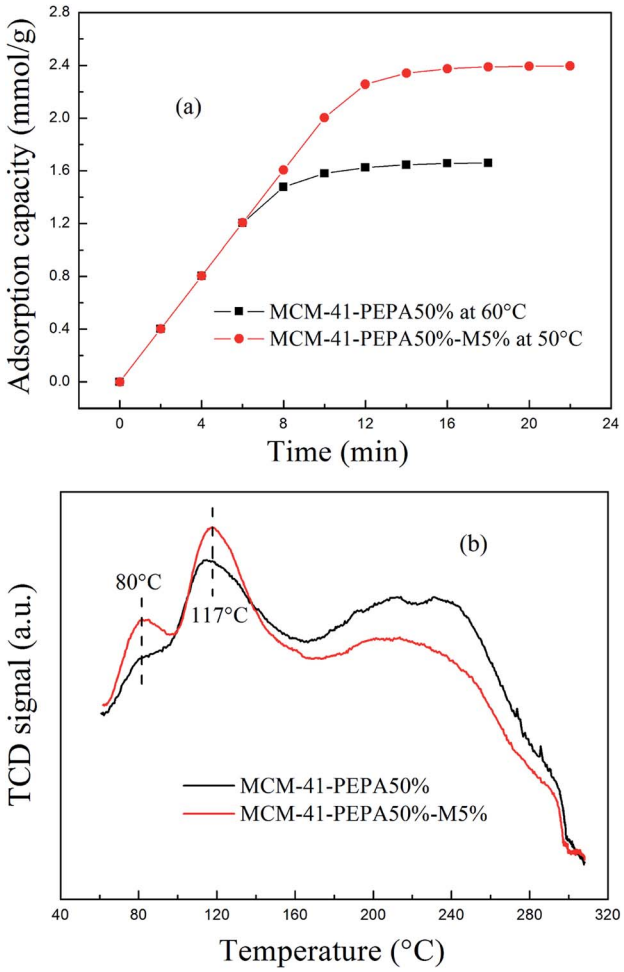

Fig. 10 The (a) adsorption rate curves and (b) TPD curves for MCM-41-PEPA50% and MCM-41-PEPA50%-M5%.

4. Conclusions

PEPA, with a similar amino density but lower price than TEPA, was found to be more suitable for preparing amine-loaded MCM-41 sorbents, in which the breakthrough and equilibrium adsorption performance as well as regenerability were found to be comparable with that for TEPA-loaded MCM-41. To improve the exposure and dispersion of viscous PEPA in MCM-41, different mass ratios of MPEG were codispersed and coimpregnated into MCM-41 to prepare composite sorbents for CO_2 capture. For 50 wt% PEPA and 5 wt% MPEG codispersed MCM-41, the breakthrough and equilibrium adsorption capacities were respectively 2.01 and 2.39 mmol g^{-1} at 50 °C, which were improved by 66% and 44% compared to the corresponding values for 50 wt% PEPA-loaded MCM-41 under the same operating conditions; after 10 regenerations, the equilibrium adsorption capacity was reduced by 5.0%, which is lower than the corresponding value of 7.8% for 60 wt% PEPA-loaded MCM-41.

The codispersed sorbent of MCM-41-PEPA50%-M5% showed a rapid breakthrough adsorption stage, with a rate of 0.20 mmol g^{-1} min^{-1}, and showed an adsorption capacity that was 84% of the equilibrium adsorption capacity, indicating a high adsorption efficiency. The CO_2-TPD results indicated that the codispersed MCM-41 contained two kinds of basic sites, with one appearing at a lower temperature, which was attributed to the synergistic hydrogen bonding interactions between PEPA and MPEG.

Conflicts of interest

There are no conflicts to declare.

Acknowledgements

The kind financial support from the Natural Science Foundation of Shandong Province (grant number ZR2017BEE038), the Foundation of State Key Laboratory of High-efficiency Utilization of Coal and Green Chemical Engineering (grant number 2017-K29), the Doctoral Research Program of Weifang University (grant number 2017BS07) and the Natural Science Foundation Joint Project of Shandong Province (grant number ZR2017LB025) is gratefully appreciated.

References

1 M. Bui, C. S. Adjiman, A. Bardow, E. J. Anthony and A. Boston, Carbon capture and storage (CCS): the way forward, *Energy Environ. Sci.*, 2018, **11**, 1062–1176.
2 S. M. Rafigh and A. Heydarinasab, Mesoporous chitosan-SiO_2 nanoparticles: synthesis, characterization, and CO_2 adsorption capacity, *ACS Sustainable Chem. Eng.*, 2017, **5**, 10379–10386.
3 L. Nie, Y. Mu, J. Jin, J. Chen and J. Mi, Recent developments and consideration issues in solid adsorbents for CO2 capture from flue gas, *Chin. J. Chem. Eng.*, 2018, **26**, 2303–2317.
4 J. Wang, L. Huang, R. Yang, Z. Zhang, J. Wu, Y. Gao, Q. Wang, D. O'Hareb and Z. Zhong, Recent advances in solid sorbents for CO_2 capture and new development trends, *Energy Environ. Sci.*, 2014, **7**, 3478–3518.
5 A. Saha, Structure-function, recyclability and calorimetry studies of CO_2 adsorption on some amine modified Type I & Type II sorbents, *Int. J. Greenhouse Gas Control*, 2018, **78**, 198–209.
6 K. Sim, N. Lee, J. Kim, E.-B. Cho, C. Gunathilake and M. Jaroniec, CO_2 adsorption on amine-functionalized periodic mesoporous benzenesilicas, *ACS Appl. Mater. Interfaces*, 2015, **7**, 6792–6802.
7 R. Veneman, N. Frigka, W. Zhao, Z. Li, S. Kersten and W. Brilman, Adsorption of H_2O and CO_2 on supported amine sorbents, *Int. J. Greenhouse Gas Control*, 2015, **41**, 268–275.
8 F. Martínez, R. Sanz, G. Orcajo, D. Briones and V. Yángüez, Amino-impregnated MOF materials for CO_2 capture at post-combustion conditions, *Chem. Eng. Sci.*, 2016, **142**, 55–61.
9 W. Li and S. Li, CO_2 adsorption performance of functionalized metal-organic frameworks of varying

topologies by molecular simulations, *Chem. Eng. Sci.*, 2018, **189**, 65–74.

10 S. Gaikwad, S.-J. Kim and S. Han, CO_2 capture using amine-functionalized bimetallic MIL-101 MOFs and their stability on exposure to humid air and acid gases, *Microporous Mesoporous Mater.*, 2019, **277**, 253–260.

11 C. Chen, N. Feng, Q. Guo, Z. Xue, L. Ding, L. Wang, H. Wan and G. Guan, Surface engineering of a chromium metal-organic framework with bifunctional ionic liquids for selective CO_2 adsorption: synergistic effect between multiple active sites, *J. Colloid Interface Sci.*, 2018, **521**, 91–101.

12 R. Huang, M. R. Hill, R. Babarao and N. V. Medhekar, CO_2 adsorption in azobenzene functionalized stimuli responsive metal-organic frameworks, *J. Phys. Chem. C*, 2016, **120**, 16658–16667.

13 M. Jia, Y. Feng, J. Qiu, X. Zhang and J. Yao, Amine-functionalized MOFs@GO as filler in mixed matrix membrane for selective CO_2 separation, *Sep. Purif. Technol.*, 2019, **213**, 63–69.

14 G. Zhang, P. Zhao, L. Hao and Y. Xu, Amine-modified SBA-15(P): a promising adsorbent for CO_2 capture, *J. CO2 Util.*, 2018, **24**, 22–33.

15 X. Wang, L. Chen and Q. Guo, Development of hybrid amine-functionalized MCM-41 sorbents for CO_2 capture, *Chem. Eng. J.*, 2015, **260**, 573–581.

16 C. Chen, S.-S. Kim, W.-S. Cho and W.-S. Ahn, Polyethylenimine-incorporated zeolite 13X with mesoporosity for post-combustion CO_2 capture, *Appl. Surf. Sci.*, 2015, **332**, 167–171.

17 G. Zhang, P. Zhao, L. Hao, Y. Xu and H. Cheng, A novel amine double functionalized adsorbent for carbon dioxide capture using original mesoporous silica molecular sieves as support, *Sep. Purif. Technol.*, 2019, **209**, 516–527.

18 X. Wang, Q. Guo, J. Zhao and L. Chen, Mixed amine-modified MCM-41 sorbents for CO_2 capture, *Int. J. Greenhouse Gas Control*, 2015, **37**, 90–98.

19 J. Cheng, Y. Li, L. Hu, J. Liu, J. Zhou and K. Cen, CO_2 absorption and diffusion in ionic liquid [P66614][Triz] modified molecular sieves SBA-15 with various pore lengths, *Fuel Process. Technol.*, 2018, **172**, 216–224.

20 C. Zhou, K. He, W. Lv, Y. Chen, S. Tang, C. Liu, H. Yue and B. Liang, Energy and economic analysis for post-combustion CO_2 capture using amine-functionalized adsorbents in a temperature vacuum swing process, *Energy Fuels*, 2019, **33**, 1774–1784.

21 M. G. Yıldız, T. Davran-Candan, M. E. Günay and R. Yıldırım, CO_2 capture over amine-functionalized MCM-41 and SBA-15: exploratory analysis and decision tree classification of past data, *J. CO2 Util.*, 2019, **31**, 27–42.

22 S. Loganathan and A. K. Ghoshal, Amine tethered pore-expanded MCM-41: a promising adsorbent for CO_2 capture, *Chem. Eng. J.*, 2017, **308**, 827–839.

23 H. Zhang, A. Goeppert, S. Kar and G. K. S. Prakash, Structural parameters to consider in selecting silica supports for polyethylenimine based CO_2 solid adsorbents. Importance of pore size, *J. CO2 Util.*, 2018, **26**, 246–253.

24 Q. Lai, Z. Diao, L. Kong, H. Adidharma and M. Fan, Amine-impregnated silicic acid composite as an efficient adsorbent for CO_2 capture, *Appl. Energy*, 2018, **223**, 293–301.

25 P. Zhao, G. Zhang, Y. Xu, Y.-K. Lv, Z. Yang and H. Cheng, Development of amine-functionalized silica foams with hierarchical pore structure for CO_2 capture, *Energy Fuels*, 2019, **33**, 3357–3369.

26 X. Li, Y. Ding, L. Guo, Q. Liao, X. Zhu and H. Wang, Non-aqueous energy-efficient absorbents for CO_2 capture based on porous silica nanospheres impregnated with amine, *Energy*, 2019, **171**, 109–119.

27 L. Mafra, T. Čendak, S. Schneider, P. V. Wiper, J. Pires, J. R. B. Gomes and M. L. Pinto, Structure of chemisorbed CO_2 species in amine-functionalized mesoporous silicas studied by solid-state NMR and computer modeling, *J. Am. Chem. Soc.*, 2017, **139**, 389–408.

28 R. Afonso, M. Sardo, L. Mafra and J. R. B. Gomes, Unravelling the structure of chemisorbed CO_2 species in mesoporous aminosilicas: a critical survey, *Environ. Sci. Technol.*, 2019, **53**, 2758–2767.

29 L. Mafra, T. Čendak, S. Schneider, P. V. Wiper, J. Pires, J. R. B. Gomes and M. L. Pinto, Amine functionalized porous silica for CO_2/CH_4 separation by adsorption: which amine and why, *Chem. Eng. J.*, 2018, **336**, 612–621.

30 X. Hou, L. Zhuang, B. Ma, S. Chen, H. He and F. Yin, Silanol-rich platelet silica modified with branched amine for efficient CO_2 capture, *Chem. Eng. Sci.*, 2018, **181**, 315–325.

31 E. S. Sanz-Pérez, T. C. M. Dantas, A. Arencibia, G. Calleja, A. P. M. A. Guedes, A. S. Araujo and R. Sanz, Reuse and recycling of amine-functionalized silica materials for CO_2 adsorption, *Chem. Eng. J.*, 2017, **308**, 1021–1033.

32 X. Wang, W. Zeng, Q. Guo, Q. Geng, Y. Yan and X. Hu, The further activation and functionalization of semicoke for CO_2 capture from flue gases, *RSC Adv.*, 2018, **8**, 35521–35527.

33 E. Vilarrasa-García, J. A. Cecilia, D. C. S. Azevedo, C. L. Cavalcante and E. Rodríguez-Castellón, Evaluation of porous clay heterostructures modified with amine species as adsorbent for the CO_2 capture, *Microporous Mesoporous Mater.*, 2017, **249**, 25–33.

34 M. Parvazinia, S. Garcia and M. Maroto-Valer, CO_2 capture by ion exchange resins as amine functionalised adsorbents, *Chem. Eng. J.*, 2018, **331**, 335–342.

35 F. Liu, S. Chen and Y. Gao, Synthesis of porous polymer based solid amine adsorbent: effect of pore size and amine loading on CO_2 adsorption, *J. Colloid Interface Sci.*, 2017, **506**, 236–244.

36 Y. Kong, G. Jiang, Y. Wu, S. Cui and X. Shen, Amine hybrid aerogel for high-efficiency CO_2 capture: effect of amine loading and CO_2 concentration, *Chem. Eng. J.*, 2016, **306**, 362–368.

37 Y. Liu, B. Sajjadi, W.-Y. Chen and R. Chatterjee, Ultrasound-assisted amine functionalized graphene oxide for enhanced CO_2 adsorption, *Fuel*, 2019, **247**, 10–18.

38 S. Lawson, C. Griffin, K. Rapp, A. A. Rownaghi and F. Rezaei, Amine-functionalized MIL-101 monoliths for CO_2 removal from enclosed environments, *Energy Fuels*, 2019, **33**, 2399–2407.

39 W. Jung, J. Park and K. S. Lee, Kinetic modeling of CO_2 adsorption on an amine-functionalized solid sorbent, *Chem. Eng. Sci.*, 2018, **177**, 122–131.
40 X. Wang, D. Wang, M. Song, C. Xin and W. Zeng, Tetraethylenepentamine-modified activated semicoke for CO_2 capture from flue gas, *Energy Fuels*, 2017, **31**, 3055–3061.
41 H. Jung, S. Jeon, D. H. Jo, J. Huh and S. H. Kim, Effect of crosslinking on the CO_2 adsorption of polyethyleneimine-impregnated sorbents, *Chem. Eng. J.*, 2017, **307**, 836–844.
42 X. Wang, W. Zeng, M. Song, F. Wang, X. Hu, Q. Guo and Y. Liu, Polyetheramine improves the CO_2 adsorption behavior of tetraethylenepentamine-functionalized sorbents, *Chem. Eng. J.*, 2019, **364**, 475–484.
43 M. B. Yue, L. B. Sun, Y. Cao, Z. J. Wang, Y. Wang, Q. Yu and J. H. Zhu, Promoting the CO_2 adsorption in the amine-containing SBA-15 by hydroxyl group, *Microporous Mesoporous Mater.*, 2008, **114**, 74–81.
44 W. Yan, J. Tang, Z. Bian, J. Hu and H. Liu, Carbon dioxide capture by amine-impregnated mesocellular foam-containing template, *Ind. Eng. Chem. Res.*, 2012, **51**, 3653–3662.
45 G. Socrates, *Infrared and Raman Characteristic Group Frequencies*, John Wiley & Sons, Chichester, UK, 2rd edn, 2001.
46 X. Wang, Q. Guo and T. Kong, Tetraethylenepentamine-modified MCM-41/silica gel with hierarchical mesoporous structure for CO_2 capture, *Chem. Eng. J.*, 2015, **273**, 472–480.
47 M. L. T. Triviño, V. Hiremath and J. G. Seo, Stabilization of $NaNO_3$-promoted magnesium oxide for high-temperature CO_2 capture, *Environ. Sci. Technol.*, 2018, **52**, 11952–11959.